

Statistical Evaporation of Rotating Clusters

F. Calvo

*Laboratoire de Physique Quantique, IRSAMC, Université Paul Sabatier,
118 Route de Narbonne, F31062 Toulouse, France*

P. Parneix

*Laboratoire de Photophysique Moléculaire, Bât. 210,
Université Paris-Sud, F91405 Orsay cedex, France.*

Unimolecular evaporation in rotating atomic clusters is investigated using phase space theory (PST) and molecular dynamics simulations. The rotational densities of states are calculated in the sphere+atom approximation, and analytical expressions are given for a radial interaction potential with the form $-C/r^p$. The vibrational densities of states are calculated using Monte Carlo simulations, and the average radial potential at finite temperature is obtained using a recent extension of the multiple range random-walk algorithm. These ideas are tested on simple argon clusters modelled with the Lennard-Jones interaction potential, at several total energies and angular momenta of the parent cluster. Our results show that PST successfully reproduces the simulation data, not only the average KER but its probability distribution, for dissociations from LJ₁₄, for which the product cluster can effectively be considered as spherical. Even for dissociations from the nonspherical LJ₈, simulation results remain very close to the predictions of the statistical theory.

I. INTRODUCTION

Fragmentation in finite systems offers a convenient way to investigate their physical and chemical properties. In this respect atomic and molecular clusters have received a great deal of attention, and experimental measurements of structural¹⁻⁷ or electronic^{8,9} data have been reported using unimolecular dissociation analyses. In particular, the relative stability of a cluster is commonly characterized by its dissociation energies, giving rise to the well known “magic numbers” in the mass spectra.¹⁰ Recently, fragmentation has been employed to probe thermodynamical properties on a more global scale, with a focus at phase transitions. Haberland and coworkers have used photoabsorption induced fragmentation to extract caloric curves in charged sodium clusters across the solid-liquid phase change.¹¹ They have also extended their measurements to probe the liquid-vapor phase change.¹² At the same time, Gobet and coworkers used event-by-event data analyses of multifragmentation in $H_3^+(H_2)_m$ clusters induced by collisions with a helium target,¹³ showing a small backbending in the caloric curve. Bréchnac *et al.* also found some evidences of the liquid-gas transition in small strontium clusters from the shape of the kinetic energy release distribution subsequent to photoexcitation.¹⁴

The possible correlations between statistical fragmentation and phase transitions have found theoretical supports in cluster physics,¹⁵⁻¹⁸ but also in nuclear physics.¹⁹ Decaying nuclei resulting from collisions²⁰ typically show features due to a very large energy deposit, where multiple fast fragments are emitted on a short time scale. In this case, the main concern is to characterize the distribution of the fragments, and the size of the remaining droplet. In suitable situations, Fisher’s formula²¹ gives a correct account of the mass distribution measured in experiments.

Atomic clusters are usually treated much more gently, by adding a small amount of excitation energy. Only a very few atoms undergo dissociation, and the evaporative process can take place over long time scales. For example, large weakly bound rare-gas clusters can exhibit extremely small rate constants if their excitation energy lies not far above the dissociation threshold, because the time required for the excitation energy to be located on the few dissociative modes rises sharply as the cluster size increases. In these systems, one is more interested by a complete characterization of the evaporation event itself, with a single ejected atom involved. Two observables carry most of the useful information, namely the dissociation rate and the kinetic energy release (KER) distribution. Weerasinghe and Amar (WA)¹⁵ theoretically investigated in great details the evaporation process in small argon clusters. Their results show that the evaporation rate, and even more the average KER, can be used as a probe of the solidlike-liquidlike phase change in the parent cluster.¹⁵ To achieve this result, they compared various statistical theories of unimolecular dissociation to the outcome of molecular dynamics (MD) simulations, below the energy range where MD becomes prohibitive. One of their conclusions is that phase space theory (PST), in the sense of Chesnavitch and Bowers,²² is able to describe accurately the full evaporation statistics in Ar_n clusters, while simpler theories such as the Rice-Ramsperger-Kassel (RRK) model²³ or the Weisskopf-Engelking formula^{24,25} only produce correct orders of magnitude.¹⁵ Some important features, including the nonlinear variation of average KER with increasing excitation energy, are completely absent from the predictions of these approximate models. Comparable methods have been applied by Peshlherbe and Hase to the dissociation in small aluminium clusters,²⁶ leading to similar conclusions.

Bréchnac and coworkers recently reported time-of-

flight mass spectrometry measurements of evaporating Na_n^+ clusters.²⁷ A careful interpretation of these results necessitated the partitioning of the translational and rotational kinetic energy released, because only the former is actually measured. The possible angular momentum of the parent cluster is a problem, since rotation can strongly alter the evaporation dynamics, hence the statistical observables. Up to now, only few theoretical works have been devoted to the dynamics of rotating clusters. Structural properties and angular momentum driven isomerizations were first investigated by Jellinek and Li.^{28–30} Using simple statistical theories, Miller and Wales further investigated static and evaporation properties on the effective rovibrational potential energy surface (PES).³¹ The influence of angular momentum on cluster thermodynamics³² and chaotic dynamics³³ also received some attention. Evaporation in rotating clusters had been previously investigated by Stace using simple models in the framework of phase space theory.³⁴ The calculations made by this author showed that angular momentum tends to increase in small clusters after evaporation (rotational heating), while it tends to decrease in large clusters (rotational cooling). These effects have been partly observed in the MD simulations performed by Weerasinghe and Amar.¹⁵

As seen from the success of phase space theory to describe evaporation in nonrotating clusters,¹⁵ it is highly desirable to extend this work to the case of finite angular momenta. This is the goal of the present paper. In the next section, we give the basic PST formalism needed to calculate the rotational density of states, in the sphere+atom approximation. Exact results are obtained for a radial interaction potential having the form $-C/r^p$, and we provide further details about the numerical implementation of the method in the more general case of a $-C/(r-r_0)^p$ interaction. The other computational ingredients include the estimation of the vibrational density of states as well as the radial interaction potential. We also carry out some MD simulations to be used as a benchmark for testing the predictions of PST. Application is made in Sec. IV to the evaporation in Ar_{14} and Ar_8 , modeled using the common Lennard-Jones potential. We finally summarize and conclude in Sec. V.

II. PHASE SPACE THEORY

In this Section, we work out the main expressions for the distribution of kinetic energy released during evaporation of rotating polyatomic molecules. Conservation of angular momentum J is rigorously included in the phase space theory.^{22,35,36} This is particularly important when treating rotating systems with prescribed values of J . Additionally, PST is built upon the hypothesis of a loose transition state, i.e. the products are the transition state. In rotating clusters, the centrifugal barrier previously explicitly considered by Miller and Wales,³¹ is naturally accounted for in PST.

Here we consider a parent cluster characterized by a rotational angular momentum J and a total rovibrational energy E . We denote by J_r the rotational angular momentum of the subcluster (product) after dissociation. Following WA and Jarrold,³⁷ the probability of finding a dissociation event with ε_{tr} kinetic energy released is given within $d\varepsilon_{\text{tr}}$ by:

$$P(\varepsilon_{\text{tr}}, E, J) = R(\varepsilon_{\text{tr}}, E, J) \left/ \int_{\varepsilon_{\text{tr}}^{\min}}^{E-E_0^{(J)}} R(\varepsilon_{\text{tr}}, E, J) d\varepsilon_{\text{tr}} \right., \quad (1)$$

with the differential rate $R(\varepsilon_{\text{tr}}, E, J)$

$$R(\varepsilon_{\text{tr}}, E, J) = R_0 \frac{\Omega_n^{(J)}(E - E_0^{(J)} - \varepsilon_{\text{tr}}) \Gamma(\varepsilon_{\text{tr}}, J)}{\Omega_{n+1}^{(J)}(E - E_r)}. \quad (2)$$

In the latter equation, R_0 is a constant factor that accounts for channel and rotational degeneracies.¹⁵ E_r is the rotational energy of the parent cluster. $\Omega_{n+1}^{(J)}$ and $\Omega_n^{(J)}$ are the vibrational densities of states (VDOS) at angular momentum J of the parent and product clusters, respectively. Γ is the rotational density of states (RDOS) of the fragments. In these notations, we have implicitly assumed that both densities of states of the product cluster depend on J , but depend only weakly on J_r . In the same line of ideas, we consider that the clusters are large enough so that the energy difference $E_0^{(J)}$ between the potential energy minima of the parent and product clusters can be taken at the same value of J for both clusters. The knowledge of the differential rate function R readily leads to the average kinetic energy released:

$$\langle \varepsilon_{\text{tr}} \rangle = \int_{\varepsilon_{\text{tr}}^{\min}}^{E-E_0^{(J)}} \varepsilon_{\text{tr}} P(\varepsilon_{\text{tr}}, E, J) d\varepsilon_{\text{tr}}. \quad (3)$$

The calculation of $P(\varepsilon_{\text{tr}}, E, J)$ and $\langle \varepsilon_{\text{tr}} \rangle$ requires one to compute both Ω and Γ for the *product* cluster, but neither the constant R_0 nor the VDOS for the parent cluster. The absolute rate constant obtained from integrating $R(\varepsilon_{\text{tr}}, E, J)$ with respect to ε_{tr} thus requires a more substantial effort than any data related to the KER. In the remainder of this section, we focus on the rotational density of states. The vibrational quantities are relatively easy to compute, and they will be dealt with later.

The calculation of the $\Gamma(\varepsilon_{\text{tr}}, J)$ function is directly linked to the energetics and angular momentum constraints during dissociation. Our main assumption will be to treat the evaporative system $\text{LJ}_{n+1} \rightarrow \text{LJ}_n + \text{LJ}$ as well represented by a sphere+atom model. Then the product cluster LJ_n has a unique rotational constant B . In this case, Chesnavitch and Bowers have shown that the rotational density of states can be calculated as²²

$$\Gamma(\varepsilon_{\text{tr}}, J) = \iint_S \Gamma(\varepsilon_r^*, J_r) dJ_r dL, \quad (4)$$

where ε_r^* stands for the upper limit of the rotational energy, L for the orbital angular momentum of the

products. The integration is carried out in the (J_r, L) plane with the boundaries \mathcal{S} discussed below. In the sphere+atom case, $\Gamma(\varepsilon_r^*, J_r)$ simply equals $2J_r$,³⁷ hence the problem is reduced to finding the expressions for the boundaries \mathcal{S} . We first consider the case of a radial dissociation potential $V(r)$ given by $V(r) = -C/r^p$, with p greater than 2.

The first boundary on \mathcal{S} is given by the constraint on the kinetic energy of the dissociating atom. The centrifugal barrier ε^\dagger that must be overcome is located at $r = r^\dagger$ such that $V_L(r) = V(r) + L^2/2\mu r^2$ is maximum. This yields

$$\varepsilon^\dagger = L^{2p/(p-2)}/\Lambda_p, \quad (5)$$

with the notation

$$\Lambda_p = \frac{2}{p-2} C^{2/(p-2)} \left(\frac{\mu p}{\hbar^2} \right)^{p/(p-2)}. \quad (6)$$

For the atom to actually dissociate, its kinetic energy must be positive at the barrier, which is expressed as

$$BJ_r^2 + L^{2p/(p-2)}/\Lambda_p \leq \varepsilon_{\text{tr}}. \quad (7)$$

The second boundary on \mathcal{S} comes from the conservation of angular momentum, $\vec{J} = \vec{J}_r + \vec{L}$, or

$$|J_r - L| \leq J \leq J_r + L. \quad (8)$$

The conditions (7) and (8) define lower and upper bounds for J_r at each value of L , denoted as $J_r^{\min}(L)$ and $J_r^{\max}(L)$, respectively. Integration over the contour \mathcal{S} can be formally carried out:

$$\Gamma(\varepsilon_{\text{tr}}, J) = \int_{L_{\min}}^{L_{\max}} [(J_r^{\max}(L))^2 - (J_r^{\min}(L))^2] dL, \quad (9)$$

where we have introduced the lower and upper bounds for the integration on L , namely L_{\min} and L_{\max} . Let now \mathcal{C} be the set of (J_r, L) points that fulfill the equation $\varepsilon_{\text{tr}} = L^{2p/(p-2)}/\Lambda_p + BJ_r^2$. Let also J_r^* and L^* be the intersection points of \mathcal{C} with the abscissa and ordinates axes, respectively. We find that

$$J_r^* = (\varepsilon_{\text{tr}}/B)^{1/2} \quad \text{and} \quad L^* = (\Lambda_p \varepsilon_{\text{tr}})^{(p-2)/2p}. \quad (10)$$

Four different cases must be treated separately, depending on whether the values of J_r^* and L^* are smaller or larger than the initial angular momentum J . These four cases are depicted in Fig. 1. They correspond to the following conditions:

- (a) $J < J_r^*$; $J < L^*$,
- (b) $J_r^* \leq J < L^*$,
- (c) $L^* \leq J < J_r^*$,
- (d) $J_r^* \leq J$; $L^* \leq J$.

In cases (a) and (c), integration starts at $L_{\min} = 0$. In cases (b) and (d), L_{\min} is determined by the intersection of \mathcal{C} with $L = J - J_r$. We denote this point by L_1 :

$$\begin{cases} L = J - J_r, \\ L^{2p/(p-2)}/\Lambda_p + BJ_r^2 = \varepsilon_{\text{tr}}. \end{cases} \quad (11)$$

In (a) and (b), $L_{\max} = L_2$ is obtained at the unique intersection of \mathcal{C} with $L = J + J_r$:

$$\begin{cases} L = J + J_r, \\ L^{2p/(p-2)}/\Lambda_p + BJ_r^2 = \varepsilon_{\text{tr}}. \end{cases} \quad (12)$$

Finally, the upper bound $L_{\max} = L_2$ is given in cases (c) and (d) by the intersection of \mathcal{C} with $L = J - J_r$, equation (11) above. Thus in (d) the two extremal values are solutions of the same equation.

At any value of L in the range $L_{\min} \leq L \leq L_{\max}$, the lower and upper values of $J_r(L)$ also depend on the conditions (a-d). For example, in case (a) one must distinguish between three subcases, namely $0 \leq L \leq L_1$, $L_1 \leq L \leq J$, and $J \leq L \leq L_2$, where L_1 denotes the intersection of \mathcal{C} with $L = J_r - J$. In the range $0 \leq L \leq J$, J_r^{\min} is equal to $J - L$. In the range $J \leq L \leq L_2$, $J_r^{\min}(L) = L - J$. The upper bound J_r^{\max} is given by $J_r^{\max} = J + L$ for $0 \leq L \leq L_1$, and by $J_r^{\max}(L) = [\varepsilon_{\text{tr}} - L^{2p/(p-2)}/\Lambda_p]/B$ for $L_1 \leq L \leq L_2$.

After some algebra, integration over the boundary \mathcal{S} leads to the total rotational density of states:

$$\begin{aligned} \Gamma(\varepsilon_{\text{tr}}, J) = & (L_2 - L_1)(\varepsilon_{\text{tr}}/B - J^2) \\ & - \frac{1}{\Lambda_p B} \frac{p-2}{3p-2} \left(L_2^{\frac{3p-2}{p-2}} - L_1^{\frac{3p-2}{p-2}} \right) \\ & + J(L_2^2 + L_1^2) - (L_2^3 - L_1^3)/3. \end{aligned} \quad (13)$$

We will not discuss the three other cases (b-d) in details, and we only provide below the final results. In cases (a) and (c), the RDOS is given by Eq. (13) above. In cases (b) and (d), it is expressed by

$$\begin{aligned} \Gamma(\varepsilon_{\text{tr}}, J) = & (L_2 - L_1)(\varepsilon_{\text{tr}}/B - J^2) \\ & - \frac{1}{\Lambda_p B} \frac{p-2}{3p-2} \left(L_2^{\frac{3p-2}{p-2}} - L_1^{\frac{3p-2}{p-2}} \right) \\ & + J(L_2^2 - L_1^2) - (L_2^3 - L_1^3)/3, \end{aligned} \quad (14)$$

which only differs from Eq. (13) by the quantity $2JL_1^2$.

We have not yet discussed the lower bound of integration on ε_{tr} in Eqn. (1) and (3), denoted as $\varepsilon_{\text{tr}}^{\min}$. This limit occurs when the curve \mathcal{C} is tangent to the line $L = J - J_r$. This condition can be cast into an equation in J_r only:

$$\frac{p-2}{p} B \Lambda_p J_r (J - J_r)^{\frac{2+p}{2-p}} = 1, \quad (15)$$

which can be easily shown to have a unique solution in the range $0 \leq J_r \leq J$. The value of $\varepsilon_{\text{tr}}^{\min}$ follows from substitution in (C) and $L = J - J_r$. In the case of a van der Waals dispersion interaction, $V(r) = -C/r^6$, the appropriate values for the rotational density of states are given exactly for $p = 6$ by

$$\begin{aligned} \Gamma(\varepsilon_{\text{tr}}, J) = & (L_2 - L_1)(\varepsilon_{\text{tr}}/B - J^2) - \frac{L_2^4 - L_1^4}{4\Lambda_6 B} \\ & + J(L_2^2 \pm L_1^2) - (L_2^3 - L_1^3)/3 \end{aligned} \quad (16)$$

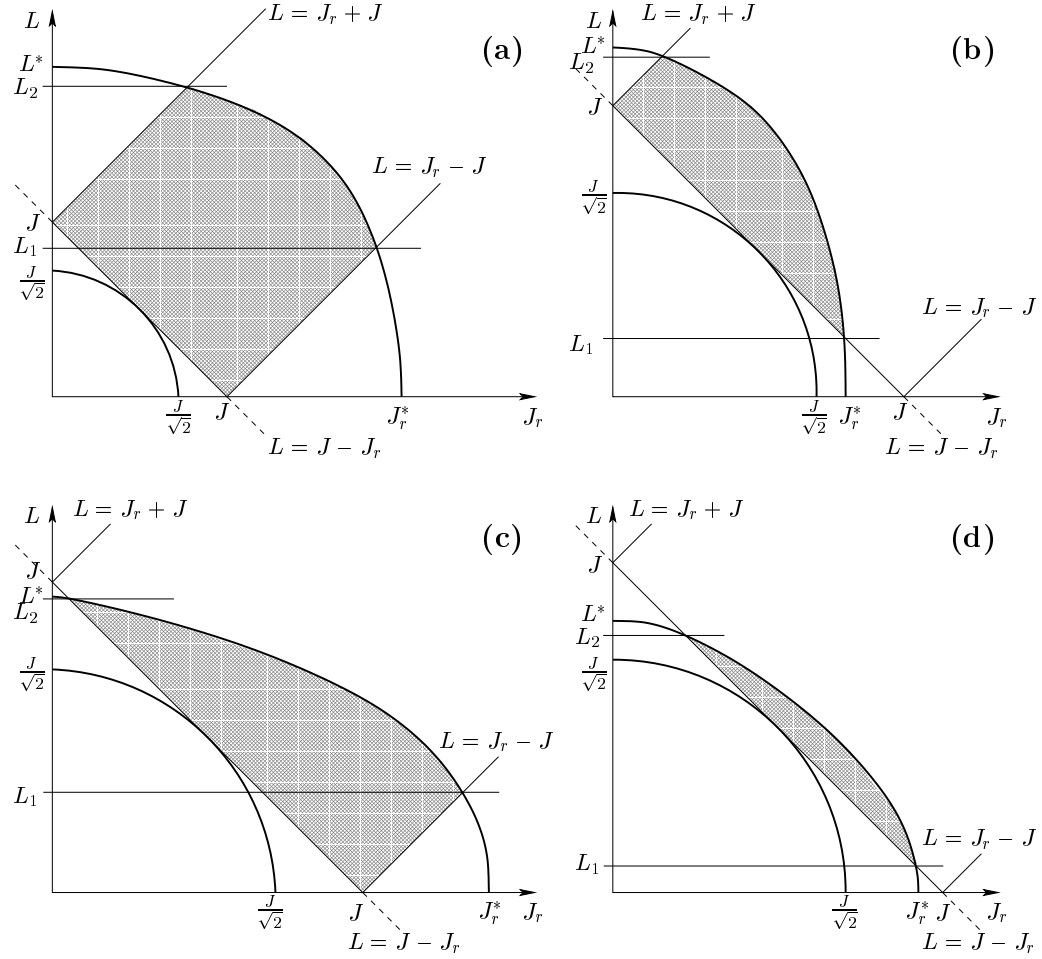


FIG. 1: Schematic representation of the (L, J_r) integration plane, denoted by \mathcal{S} in the text. (a) $J < L^*$ and $J < J_r^*$; (b) $J_r^* \leq J < L^*$; (c) $L^* \leq J < J_r^*$; and (d) $J > L^*$ and $J > J_r^*$. The outer boundary is defined by the curve \mathcal{C} (see text), the inner boundary is the circle with radius J centered at $(0,0)$.

where the plus sign stands in cases (a) and (c), and the minus sign stands in (b) and (d). In the case $p = 6$, an analytical expression for $\varepsilon_{\text{tr}}^{\text{min}}$ can also be found

$$\varepsilon_{\text{tr}}^{\text{min}} = BJ^2 + \frac{2}{3}B^2\Lambda_6J + \frac{2}{27}B^3\Lambda_6^2 - \left(\frac{2}{27}B^3\Lambda_6^2 + \frac{4}{9}B^2\Lambda_6J \right) \left(1 + \frac{6J}{B\Lambda_6} \right)^{1/2} \quad (17)$$

which is given in the low J regime by $\varepsilon_{\text{tr}}^{\text{min}} = J^3/\Lambda_6$, up to the fourth order in J . The numerical implementation of the above formulas is straightforward. At fixed total energy E and angular momentum J of the parent cluster, one must first calculate the lower and upper limits $\varepsilon_{\text{tr}}^{\text{min}}$ and $\varepsilon_{\text{tr}}^{\text{max}} = E - E_0^{(J)}$. For each value of ε_{tr} in this range, equations (11) and (12) must be solved numerically to give L_1 and L_2 , and the rotational density of states is calculated using Eqn. (13) and (14) above.

All the previous formalism has been derived by assuming an interaction potential with the form $V(r) = -C/r^p$. It turns out that this expression does not give a very good account of the finite extension of the cluster, and that a better representation of the atom-cluster interaction is provided by $V(r) = -C/(r - r_0)^p$, with $r_0 > 0$. In this case, and more generally for an arbitrary form of $V(r)$, the computation of the rotational density of states must be carried out numerically. Firstly, for a series of L , the location $r^*(L)$ of the centrifugal barrier is obtained by solving

$$\left. \frac{\partial V}{\partial r} \right|_{r=r^*} = \frac{L^2}{\mu(r^*)^3}. \quad (18)$$

One then deduces the height $\varepsilon^\dagger(L)$ of the barrier:

$$\varepsilon^\dagger(L) = \frac{L^2}{2\mu(r^*)^2} - V(r^*). \quad (19)$$

At a given ε_{tr} , the integration boundaries \mathcal{S} become

$$\begin{cases} \varepsilon^\dagger(L) + BJ_r^2 \leq \varepsilon_{\text{tr}}, \\ |J_r - L| \leq J \leq J_r + L \end{cases} \quad (20)$$

and the limits L_1 and L_2 are still given by equations (2) and (3) after replacing $L^{2p/(p-2)}/\Lambda$ by $\varepsilon^\dagger(L)$. While $(J_r^{\text{min}})^2$ is still equal to $(J - L)^2$, $(J_r^{\text{max}})^2$ is now obtained from $[\varepsilon_{\text{tr}} - \varepsilon^\dagger]/B$ in the range $L_1 \leq L \leq L_2$. The integration of $\Gamma(\varepsilon_{\text{tr}}, J)$ must be done numerically, after estimating $\varepsilon_{\text{tr}}^{\text{min}}$ from the tangency condition of $\varepsilon_{\text{tr}} = \varepsilon^\dagger + BJ_r^2$ with $L = J_r - J$.

III. COMPUTATIONAL PROCEDURE

A. Vibrational density of states

The vibrational densities of states $\Omega^{(J)}(E)$ depend implicitly on the total angular momentum \vec{J} of the cluster.

Actually this dependence acts by two ways.³² Firstly, the centrifugal effects perturb the potential energy surface into an effective, rovibrational surface.^{28,31} Secondly, the conservation of the vector \vec{J} adds an extra geometrical weight in the configurational density of states or in the partition function. This weight is given explicitly by $1/\sqrt{\det \mathbf{I}}$, where \mathbf{I} is the inertia tensor at the current configuration.^{32,39} The angular momentum is naturally conserved in constant energy molecular dynamics simulations, as well as in constant temperature Nosé-Hoover schemes at $\vec{J} = \vec{0}$, but not in conventional Monte Carlo simulations. Therefore, some differences between the MD and MC procedures may arise when this weight may span several orders of magnitude, as in the case of Ar_3^+ , which is linear in its ground state geometry.⁴⁰

To calculate $\Omega^{(J)}(E)$ for several values of J , we have used the Monte Carlo method proposed in Ref. 32, further improved with the parallel tempering accelerating scheme.⁴¹ The multiple histogram method⁴² was then used to estimate the configurational densities of states. In turn, the total vibrational densities of states were obtained from the configurational densities by a simple convolution product.

The present results were checked by performing additional molecular dynamics simulations. The histogram analysis³⁸ showed a good agreement between the MC and the MD calculation. We have also checked the physical relevance of the calculation by computing other related thermodynamical observables, such as the canonical heat capacity. At low values of \vec{J} , the melting temperature was seen to roughly decrease with \vec{J} as J^2 , in agreement with previous works.³²

B. Radial potential

In a first approach, the dissociation potential $V(r)$ felt by an atom leaving the n -atom Lennard-Jones cluster can be approximated by its asymptotic form $-C_6^{(n)}/r^6$. At very large distances r , the $C_6^{(n)}$ parameter is given by $4n\varepsilon\sigma^6$ LJ units. However, at intermediate distances, where the centrifugal barrier is likely to be located, the finite extent of the cluster induces significant deviations of the average potential. A simple approach to this problem is to consider a continuous homogeneous distribution of Lennard-Jones centers inside a sphere of radius $R \propto n^{1/3}$. For large sizes, this leads to the Gspann-Vollmar potential V_n .⁴³

$$V_n(r) = C_{12} \frac{r^6 + 21r^4r_0^2/5 + 3r^2r_0^4 + r_0^6/3}{(r^2 - r_0^2)^9} - \frac{C_6}{(r^2 - r_0^2)^3}, \quad (21)$$

where C_{12} , C_6 and r_0 are size-dependent and given by

$$\begin{aligned} C_{12} &= 4n\varepsilon\sigma^{12}; \\ C_6 &= 4n\varepsilon\sigma^6; \end{aligned} \quad (22)$$

$$r_0 = (3/p\pi\rho)^{1/3}[n^{1/3} - 1]. \quad (23)$$

In the above equation, ρ is the atomic density in the solid state. The Gspann-Vollmar potential was built in a similar way as the Girifalco potential describing the interaction between C_{60} molecules.⁴⁴ It is not appropriate for medium-size, nonspherical clusters, or for intermediate distances r , where the continuous approximation would break down. In addition, because the cluster is thermalized at a finite temperature, the atomic fluctuations may induce some changes in the average potential felt by the tagged distant atom. Using constraint dynamics, Weerasinghe and Amar¹⁵ showed that the simple $-C_6/r^6$ form was not fully appropriate to describe the atom-cluster interaction, and that a much better fit was obtained using the $-C_6/(r-r_0)^6$ form. The Gspann and Vollmar results also suggest that a $-C_6/(r^2 - r_0^2)^3$ form could also be used. We have carried out some constrained Monte Carlo simulations at finite temperature, by keeping the external atom at a fixed distance r from the cluster center of mass. The temperature effects were not investigated in the paper by Weerasinghe and Amar, and we have chosen to perform the calculation at low (0.01 LJ units) and high T , namely $T = 0.2$ for LJ_8 and $T = 0.3$ for LJ_{14} . These values are close to the melting points of the two clusters, above which evaporation takes place in a sub-nanosecond time scale.

As an alternative to the MC simulations with constraints, we have calculated the finite temperature dissociation potential using the recently proposed multiple range random walk algorithm by Wang and Landau.⁴⁵ This method has been straightforwardly extended to the computation of effective potentials and potentials of mean forces,⁴⁶ and consists of performing a Metropolis Monte Carlo simulation using the following acceptance rule:

$$\text{acc}(\mathbf{R}_{\text{old}} \rightarrow \mathbf{R}_{\text{new}}) = \min \left[1, \frac{g(r_{\text{old}})}{g(r_{\text{new}})} \exp \{-\beta[V(\mathbf{R}_{\text{new}}) - V(\mathbf{R}_{\text{old}})]\} \right], \quad (24)$$

where $\beta = 1/k_B T$, \mathbf{R}_{old} and \mathbf{R}_{new} are two successive points in the configuration space, r_{old} and r_{new} the corresponding atom-cluster distances, respectively. $g(r)$ is a weight function, initially set to 1 in the entire range of r , which evolves dynamically along the MC simulation by the operation $g(r) \rightarrow f \times g(r)$ after the distance r has been visited. The constant factor f is initially set to 2, and gradually decreases to 1 after a given number of Monte Carlo steps. After several iterations of this process, the function $\Gamma(r) = -\beta^{-1} \ln g(r)$ converges to the potential of mean force (PMF) $W(r)$.⁴⁶

$$\Gamma(r) \rightarrow W(r) = -\beta^{-1} \ln p(r), \quad (25)$$

where $p(r)$ is the probability distribution of finding the atom at the distance r from the cluster, given by the canonical average $p(r_0) = \langle \delta[r_0 - r(\mathbf{R})] \rangle$.

Once the PMF is known, it can be subsequently used in a biased multicanonical simulation to sample the entire

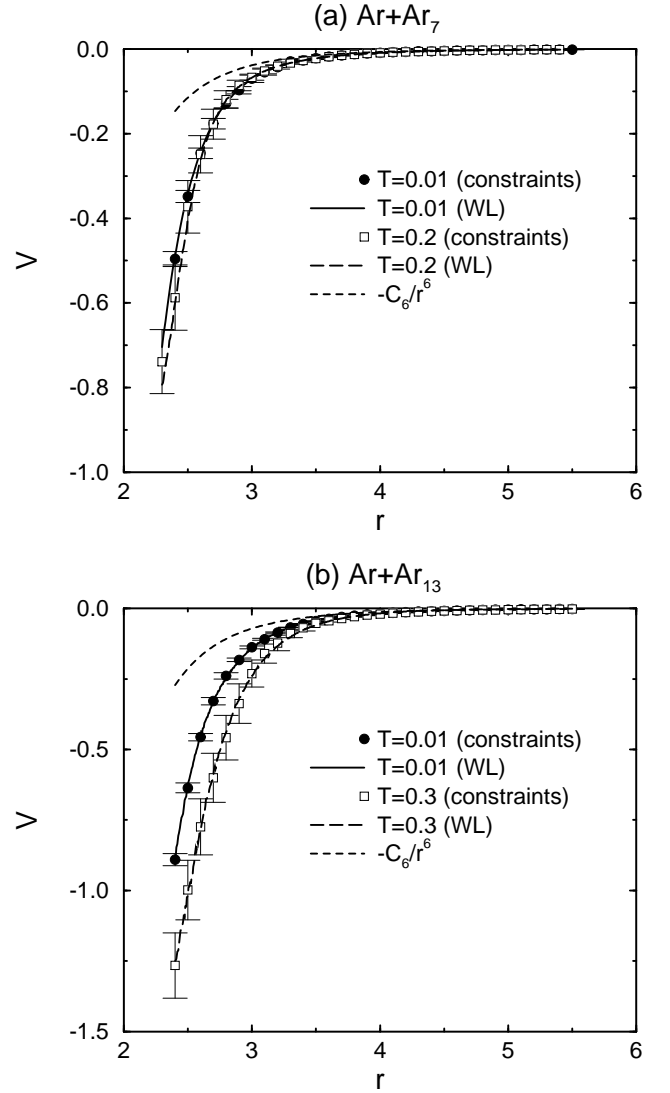


FIG. 2: Atom-cluster radial potential in the reaction $LJ_{n+1} \rightarrow LJ_n + LJ$. The symbols are from constrained MC simulations, the solid and long dashed lines are the result of the Wang-Landau (WL) multicanonical reweighting scheme. The asymptotic law $-C_6/r^6$, with $C_6 = 4n$ LJ units, is also drawn as a dashed line. The data are plotted for two temperatures in each case. (a) $n = 7$; (b) $n = 13$.

range of distances in a uniform way. For this we replace the potential V by $V + W$. The average potential $V(r)$ felt by the atom at distance r from the cluster center of mass is given by the usual reweighting formulas.⁴⁷ The Wang-Landau scheme allows one to compute the potential V over a continuous range of r , instead of only a small set when using constraint dynamics.

We have represented in Fig. 2 the effective potential calculated from constrained MC simulations and from multicanonical simulations for the two sizes $n+1 = 8$ and $n+1 = 14$, at low and high temperatures. In each case, we observe a very good agreement between the two meth-

ods, suggesting that the Wang-Landau/multicanonical scheme can yield accurate average potentials over continuous range of distances. For the two clusters, the interaction between the external atom and the cluster is stronger at higher temperature. This can be explained by the larger “volume” of the cluster in its liquidlike state with respect to its solidlike low temperature value. Hence the apparent extent of the cluster is larger, and the potential is larger in modulus. As can be seen in the two pannels of Fig. 2, the asymptotic $-C_6/r^6$ form is not appropriate at intermediate distances when taking $C_6 = 4n\epsilon\sigma^6$. As noted by Weerasinghe and Amar,¹⁵ setting this constraint on C_6 free does not improve the behavior of $V(r)$ much. A better fit is obtained with the expression $V(r) = -C_6/(r - r_0)^6$. The values of C_6 and r_0 as a function of cluster size and temperature are given in Table I.

TABLE I: Fitting parameters C_6 and r_0 of the average atom-cluster LJ potential $V(r) = -C_6/(r - r_0)^6$, and average rotational constant B , for LJ_n clusters at different temperatures.

Cluster size n	Temperature (ϵ/k_B)	C_6 ($\epsilon\sigma^6$)	r_0 (σ)	B ($m\sigma^2$)
7	0.01	8.070	0.809	0.150
7	0.20	8.728	0.802	0.135
13	0.01	19.149	0.733	0.0534
13	0.30	62.353	0.499	0.0444

Temperature effects are weak on the smaller cluster, as both C_6 and r_0 remains nearly constant. This is probably due to the fact that, upon melting, the non spherical LJ_7 cluster does not really enlarge, but instead visits other (still non spherical) isomers. On the other hand, a significant change is seen on the parameters for the much more spherical $n = 13$. At large temperature, the values we get are found to yield a very similar average potential than the one found by Weerasinghe and Amar.¹⁵ However, because these authors employed constant energy MD simulations and because they did not provide the total energy used for this cluster, we cannot reliably compare our results with theirs.

We now have all the ingredients required for the PST calculations. In order to assess or question the quality of the statistical theory, we need to carry out simulations of the actual evaporation process at finite angular momentum.

C. Molecular dynamics simulation of the evaporation dynamics

For each size and for each value of angular momentum, we have considered a set of 5000 molecular dynamics trajectories. The average kinetic energy release has been analysed after each trajectory ending into an evaporation event. The two contributions of the KER were evaluated, namely the rotational part of the product LJ_n subcluster,

and the translational contribution of the external atom undergoing evaporation. The instant of evaporation was considered as the last time at which the radial velocity of the atom was negative.¹⁵ By varying the total angular momentum between $J = 0$ and $J \approx 5$ LJ units,⁴⁸ we have performed a systematic study of the effects of rotation on the evaporation process.

IV. RESULTS AND DISCUSSION

In this paper, we will focus on the energetics of the unimolecular process, rather than on the absolute evaporation constant. This choice is mainly guided from previous studies where the relationship between phase transition in the product clusters and the evaporation statistics was most clearly evidenced on the kinetic energy released.^{15–17} Two different unimolecular reactions have been considered, involving the nearly spherical LJ_{13} product and the nonspherical LJ_7 system. This latter cluster has an ellipsoidal symmetry with inertia momenta in the ratio (0.64,0.64,1) at $T = 0$. The two reactions studied here are thus $\text{LJ}_{14} \rightarrow \text{LJ}_{13} + \text{LJ}$ and $\text{LJ}_8 \rightarrow \text{LJ}_7 + \text{LJ}$.

A. $\text{LJ}_{14} \rightarrow \text{LJ}_{13} + \text{LJ}$

LJ_{13} is a magic cluster and shows enhanced melting point and latent heat of melting with respect to its immediate neighbors LJ_{12} and LJ_{14} . In addition to its spherical shape, this cluster provides a good candidate for investigating the melting transition as seen from its evaporation observables.

To apply the PST formalism, we first have to calculate the rotational density of states $\Gamma(\epsilon_{\text{tr}}, J)$ for different values of the angular momentum J . As explained in Section II, $\Gamma(\epsilon_{\text{tr}}, J)$ is sensitive to the radial potential $V(r)$ felt by the dissociating atom. It is also sensitive to the rotational constant B of the product LJ_{13} cluster. In Fig. 3, $\Gamma(\epsilon_{\text{tr}}, J)$ is plotted for $J=0, 2$, and 4 using the radial potential $-C_6/(r - r_0)^6$ and the rotational constant calculated at moderate temperature, $T = 0.3$, close to the melting point. The parameters are given in Table I. For comparison, we have also plotted the RDOS calculated using the simpler radial potential $-C_6/r^6$, with $C_6 = 4n$ and the rotational constant at $T = 0$. The latter potential does not fully reproduce the simulated potential, but the asymptotic limit (large r) is known to be exact. Because the discrepancy between the two radial potentials is quite large, the significant differences between the predictions of PST in the rotational densities show that the centrifugal barriers are indeed located within the range of distances plotted in Fig. 2. The PST calculation using the analytical results at $r_0 = 0$ notably underestimates the RDOS, by about 15% for any J and ϵ_{tr} . The effects of a finite angular momentum in the parent cluster are strong. The value of ϵ_{tr} at which Γ sharply increases,

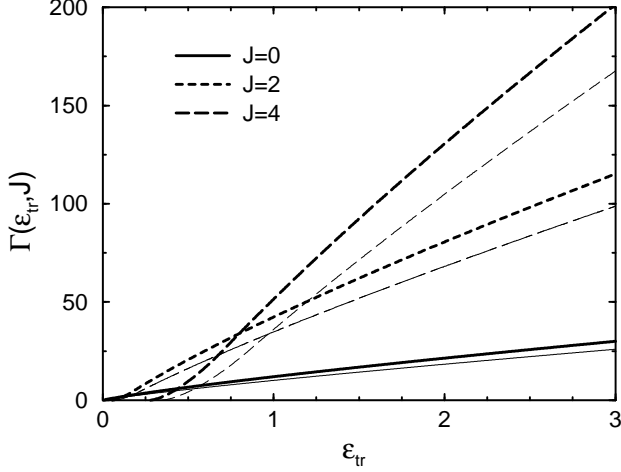


FIG. 3: Rotational density of states $\Gamma(\epsilon_{tr}, J)$ as a function of ϵ_{tr} for 3 values of J in the unimolecular dissociation of LJ_{14} . The curves plotted are the predictions of PST using the simulated radial potential at $T = 0.3$ (thick lines) or the simpler $-C_6/r^6$ potential with $C_6 = 52$ (thin lines).

previously denoted as ϵ_{tr}^{\min} , clearly changes with J . Moreover, the slope of the RDOS also increases with J . As a consequence, there is an order of magnitude increase at $\epsilon_{tr} = 3$ between $J = 0$ and $J = 4$. This latter value can be considered as still moderate for LJ_{14} , as there is only a small variation in the potential energy surface, and in the related properties such as the heat capacity.^{31,32} In particular, the cluster structure is only slightly perturbed, and spontaneous isomerization is not expected to take place below about 15 LJ units.²⁹

In Fig. 4 we have represented the results of the molecular dynamics simulations to be used as benchmarks for the present theoretical analyses. The rotational, translational and total kinetic energy released are plotted as a function of J for two different total energies of the parent cluster. The effect of J on the energetics of the dissociation reaction is mainly governed by the evolution of the rotational contribution of the KER. Around $J = 4$, this contribution becomes larger than the translational energy. This latter contribution appears almost constant up to $J \sim 4$ and slightly increases at higher J . In the range of energies considered here, the effect of internal energy is weak. We observe a steady increase in the energies released during evaporation as both angular momentum and internal energy increase, as intuition would suggest.

In the form detailed above, phase space theory only gives us access to the total (translational+rotational) kinetic energy released. We have plotted in Fig. 5 the variations of the average KER $\langle \epsilon_{tr} \rangle$ calculated from MD simulations as a function of J , and compared them to the predictions of PST in the following three approxima-

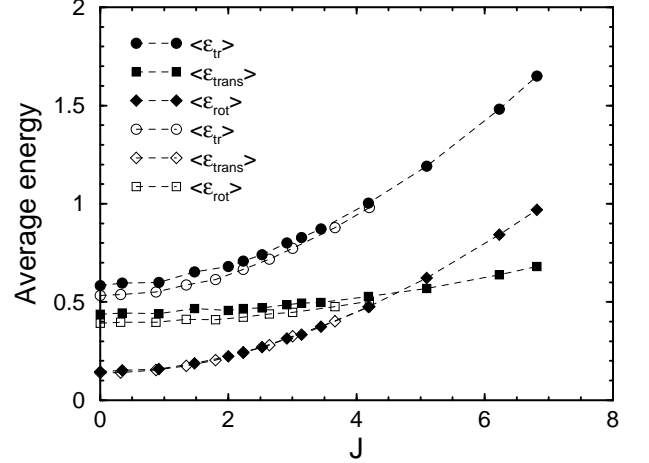


FIG. 4: Average translational ($\langle \epsilon_{trans} \rangle$, squares), rotational ($\langle \epsilon_{rot} \rangle$, diamonds) and total ($\langle \epsilon_{tr} \rangle$, circles) kinetic energies released as a function of J in the dissociation of LJ_{14} at $E = -26$. All results are from MD simulations. Full symbols correspond to $E = -26$; empty symbols are for $E = -29$.

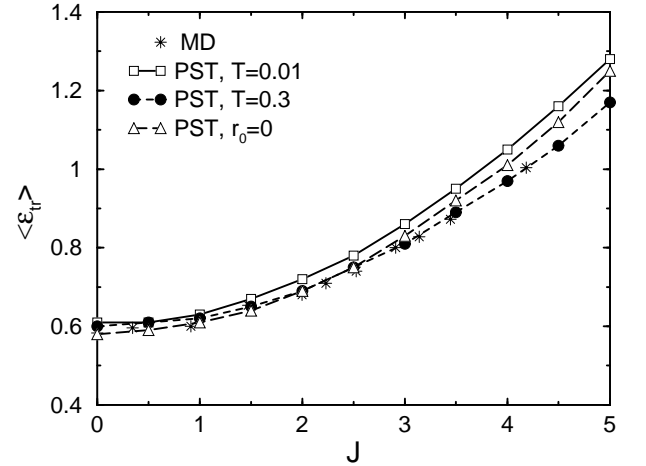


FIG. 5: Average total kinetic energy release in the dissociation of LJ_{14} as a function of angular momentum J at $E = -26$. Comparison between MD simulation and phase space theory using different radial potentials.

tions. The radial potential was either taken with $r_0 = 0$ or with finite r_0 , and in the latter case, two temperatures were taken, corresponding to either the rigid case ($T = 0.01$) or to the liquid case ($T = 0.30$). The values of the parameters r_0 , C_6 and B implicitly depend on these approximations. As can be seen from Fig. 5, all three approximations perform quite well. Looking more closely, we notice that the PST calculation at low temperature

overestimates $\langle \varepsilon_{\text{tr}} \rangle$, and that the approximation $r_0 = 0$ leads to a slightly diverging KER above $J \sim 3$. Actually, only the calculation at finite r_0 and temperature close to the melting point remains quantitatively close to the simulation data in the entire range of E . This is not so surprising, because the simulation takes place at rather large internal energies, where the cluster is in a liquid-like state. At low temperature, the average rotational constant is larger (see Table I). Therefore the rotational contribution to ε_{tr} is overestimated, which explains the relatively high values of $\langle \varepsilon_{\text{tr}} \rangle$ in Fig. 5. Another possible cause could be the less attractive interaction potential at this low temperature (see the lower panel of Fig. 2), resulting in higher centrifugal barriers, hence a further shift of ε_{tr} to a larger value.

The variations of the average KER as a function of internal energy are displayed in Fig. 6 for the same three values of angular momentum, $J = 0$, $J = 2$, and $J = 4$ LJ units. The results of the PST calculations are represented in the energy range where an inflection occurs due to the melting phase change in LJ₁₃.¹⁵ The excitation energy where this inflection takes place show a weak dependence over the radial potential used, as well as a nearly constant value with increasing J . As angular momentum increases, the average KER also increases, following the expected scaling law $\langle \varepsilon_{\text{tr}} \rangle (J > 0) \approx \langle \varepsilon_{\text{tr}} \rangle (J = 0) + aJ^2$. Looking now at the differences between the PST calculations, we notice that the use of the $-C/r^6$ radial potential overestimates the average energy released, more and more as J increases. This quantitative difference can be explained from the differences in the RDOS, as seen in Fig. 3. For excitation energies $E/n \sim 1$, $\langle \varepsilon_{\text{tr}} \rangle$ is less than about 1. In this range, the energy shift $\varepsilon_{\text{tr}}^{\text{min}}$ plays a crucial role, and its overestimation with the $r_0 = 0$ approximation is consistent with the larger average kinetic energy released in Fig. 6.

Because Fig. 5 does not confidently discriminates between the various approximations used in our application of PST, we turn to the probability distribution of ε_{tr} at given total energy and angular momentum of the parent cluster, which carries more precise information. In Fig. 7 we have represented these distributions obtained from MD simulations and from PST, with the two radial potentials either with $r_0 = 0$ and $C_6 = 4n$ or with the potential extracted from simulations close to the melting point. The results are given for $J = 0$ and $J = 5$ LJ units. As can be observed on the upper panel of this figure, the agreement between MD and PST is excellent at $J = 0$, and the two PST calculations give very similar data. The rotational density of states roughly shows linear variations upon increasing ε_{tr} in Fig. 3. We also show in Fig. 5 the probability densities computed using the explicit linear approximation $\Gamma(\varepsilon_{\text{tr}}, J) = \alpha(\varepsilon_{\text{tr}} - \varepsilon_{\text{tr}}^{\text{min}})$. Actually the slope constant α does not play any role in the KER distribution. This linear Weisskopf-like behavior²⁴ leads to slight shift of the distribution toward higher energies.

A nonzero angular momentum appears as a more strin-

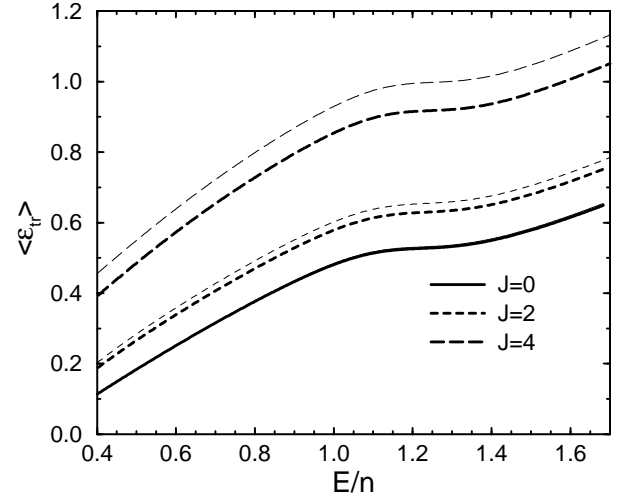


FIG. 6: Average total kinetic energy release in the dissociation of LJ₁₄ as a function of E/n for 3 values of the initial angular momentum J , from the predictions of PST using the simulated radial potential at $T = 0.3$ (thick lines) or the simpler $-C_6/r^6$ potential with $C_6 = 52$ (thin lines).

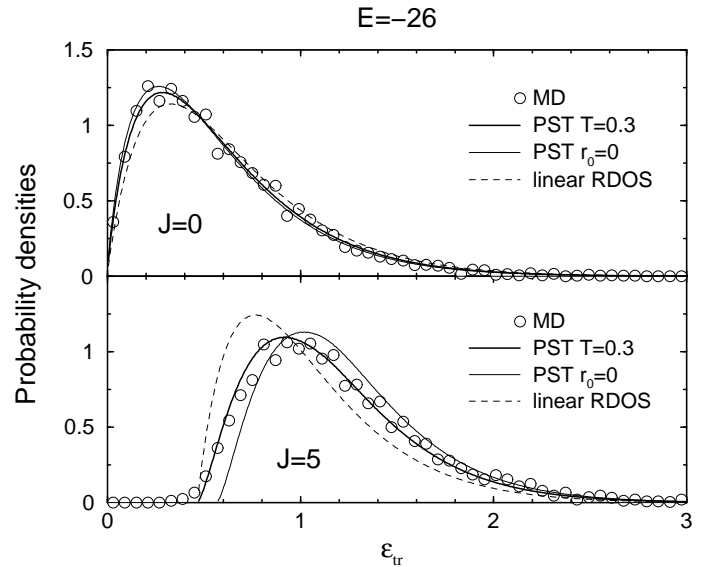


FIG. 7: Probability distributions of the total kinetic energy release ε_{tr} at $E = -26$ for two values of J , in the dissociation of LJ₁₄: (a) $J=0$; (b) $J=5$. The dashed lines refer to the linear approximation $\Gamma(\varepsilon_{\text{tr}}, J) \propto \varepsilon_{\text{tr}} - \varepsilon_{\text{tr}}^{\text{min}}(J)$.

gent test for the statistical theory, as we see on the lower panel of Fig. 7 that the agreement between MD and PST is significantly better with the calculation performed using the radial potential corresponding to $T = 0.3$. This is consistent with the better agreement previously observed in Fig. 4. In particular, the threshold value $\varepsilon_{\text{tr}}^{\text{min}}$ of ε_{tr} at which the probability suddenly rises (near $\varepsilon_{\text{tr}} \sim 0.5$ LJ unit) is well reproduced by PST at $T = 0.3$, but is not

in the approximation $r_0 = 0$. Evaporations from rotating clusters are characterized by a nonzero value of this threshold, which is due to the extra excitation energy needed for the system to overcome the larger centrifugal barrier. The influence of the shape of the rotational density of states on the probability distribution of ε_{tr} is also investigated using the linear approximation. The difference with previous PST calculations is more significant, which indicates the strong influence of the shape of the RDOS in the vicinity of $\varepsilon_{\text{tr}}^{\text{min}}$.

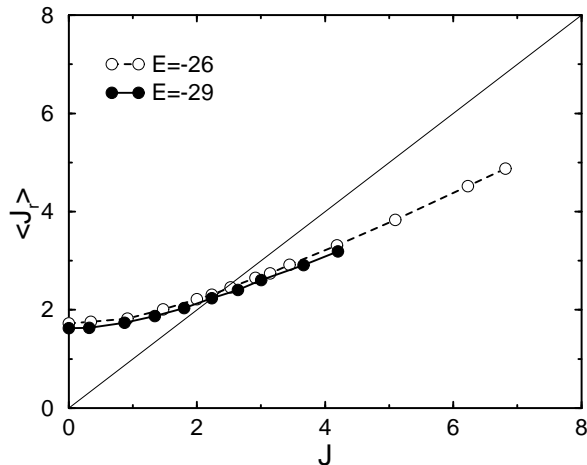


FIG. 8: Average angular momentum of the product subcluster as a function of the initial angular momentum J of the parent LJ_{14} , from MD simulations at two total energies.

Finally, we have represented in Fig. 8 the average final angular momentum J_r of the product cluster as a function of the initial J , at two total internal energies, from molecular dynamics simulations. On this figure the line $J_r - J = 0$ is also drawn. Depending on the initial angular momentum, the product cluster can gain or lose some of its rotational velocity. These rotational cooling and rotational heating effects occur for $J \lesssim J_0 = 2.3$ LJ units and $J \gtrsim J_0$, respectively. The threshold value J_0 weakly depends on the total internal energy, in the rather limited range investigated here.³⁴ This can be understood using the following simple arguments. At low J , evaporating an atom induces an orbital momentum \vec{L} , which is nearly balanced by the angular momentum \vec{J}_r . Hence angular momentum increases for initially small values of J . On the other hand, rapidly rotating clusters lose a part of their angular velocity by emitting one atom, and J tends to decrease upon evaporation.

B. $\text{LJ}_8 \rightarrow \text{LJ}_7 + \text{LJ}$

We now turn to the evaporation statistics in the smaller LJ_8 cluster. The product cluster LJ_7 is nonspher-

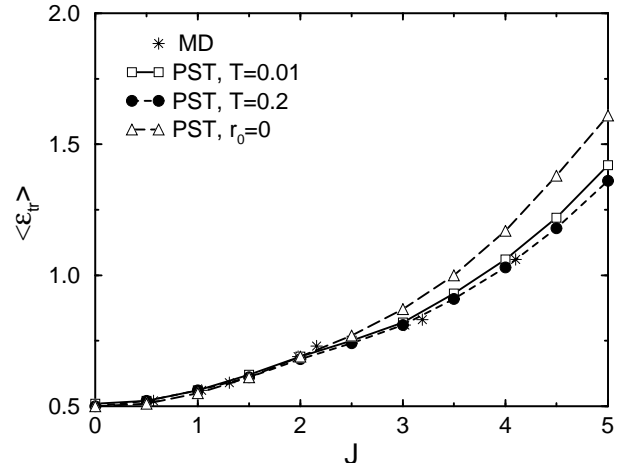


FIG. 9: Average total kinetic energy release in the dissociation of LJ_8 as a function of angular momentum J at $E = -10.21$. Comparison between MD simulation and phase space theory using different radial potentials.

ical not only in its lowest energy structure, but also in any of his three other stable isomers. The average kinetic energy released during dissociation is represented in Fig. 9 versus the total angular momentum of the parent cluster J . The values plotted are the results of MD simulations as well as the predictions of PST under various approximations concerning the radial potential. As in the previous paragraph, we have considered the simple $-C_6/r^6$ case with $C_6 = 4n$, and two more realistic potentials extracted from Monte Carlo simulations at $T = 0.01$ and $T = 0.2$, respectively. The latter value is close to the isomerization point in this system. The effective rotational constant was taken as the average over the different instantaneous values at the corresponding temperatures. They are also given in Table I. As in Fig. 5, the general agreement between MD and PST is good, but we notice that the discrepancy is larger for the PST calculation with $r_0 = 0$. The effect of temperature on the radial potential is weak in this case. This may be partly due to the lower melting point of this system, but should be correlated with the similar radial potentials felt by the leaving atom, as represented in Fig. 2.

The probability distribution of kinetic energy released is reported in Fig. 10 at the total energy $E = -10.21$ LJ units, and at zero or nonzero angular momentum of the parent cluster. As was the case for the bigger cluster, PST reproduces very accurately the results of MD simulations at $J = 0$, and the two calculations with the different radial potentials yield essentially similar data. In contrast, the distributions at $J = 3$ differs somewhat from the simulation results. In particular, the general shape predicted by PST is too sharp with respect to MD, and the value of ε_{tr} where the probability starts

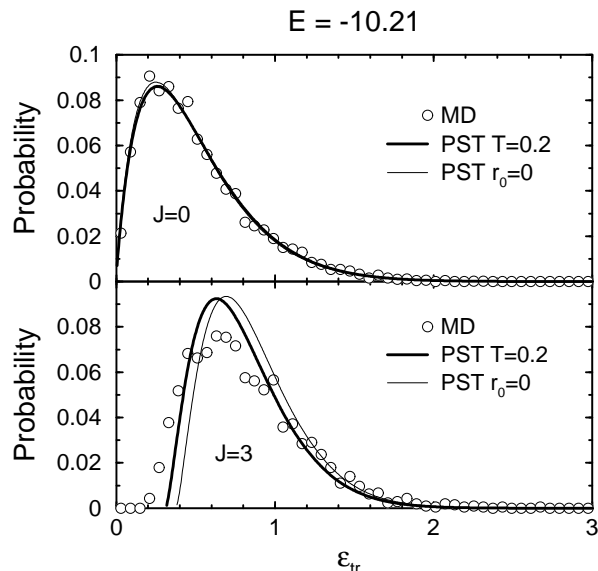


FIG. 10: Probability distributions of the total kinetic energy release ε_{tr} at $E = -10.21$ for two values of J , in the dissociation of LJ_8 : (a) $J=0$; (b) $J=3$.

to increase is too high by about 50%. This error further increases when using the alternative radial potential corresponding to $r_0 = 0$. The discrepancies observed here should be mainly due to the erroneous assumption of a spherical product.

Nevertheless, the global behaviors of both the KER and its probability distribution remain correctly reproduced by phase space theory, indicating that this statistical approach captures all the important physical and chemical ingredients of unimolecular dissociation in weakly bound systems, especially the conservation of angular momentum.

V. CONCLUSION

Unimolecular decay in large atomic systems is easily treated using simple theories such as the RRKM or Weisskopf-Engelking statistical approaches. Phase space theory not only includes possible anharmonic effects, but also the rigorous constraints on angular momentum, through general expressions for the differential rates of dissociation. Weerasinghe and Amar¹⁵ were the first to show clearly that PST is qualitatively and quantitatively accurate in predicting rate constants and energetic distributions in the evaporation of nonrotating atomic clusters.

Building upon their seminal paper, we have extended their work to the more general case of a finite angular momentum in the parent cluster. For this we calculated exactly the rotational density of states in the case of an interaction between the product cluster and the dissociating atom having the form $-C/r^p$. The implementation to other forms has also been given. The anharmonic vibrational densities of states were calculated using Monte Carlo simulations on the effective rovibrational energy surface,³² and the radial potential was calculated using an extension of the recent Wang-Landau algorithm.^{45,46}

We have tested the applicability of PST to the case of unimolecular evaporation in the LJ_{14} and LJ_8 clusters. These two different cases allow us to question the hypothesis of a sphere+atom collision underlying the statistical formalism. We have shown that PST was quantitatively accurate in predicting the distribution and average value of the kinetic energy released during dissociation, especially after considering the radial potential calculated at temperatures close to the melting point, where dissociation actually occurs on the time scale of MD. Taking the simple form $-C/r^6$ introduces some extra errors, in particular at large energies and angular momenta. We have also seen that dissociation in LJ_8 was less well described using PST in the sphere+atom assumption. Beyond this approximation, one could generalize the present formalism to the case of ellipsoid or even triaxial shapes. Extension to molecular systems is also possible, provided that the internal degrees of freedom of the dissociating molecule are correctly accounted for.

To bridge the gap between the results obtained in the present work and the experimental concerns, one must extract the separate translational and rotational contributions to the total kinetic energy released during evaporation. This separation was achieved previously in the case of nonrotating parent clusters.⁴⁹ As a first step, it would be useful to extend the present effort to the characterization of the angular momenta distribution after dissociation of an initially rotating system. The starting distribution of J could there be either a delta function (as in the present work) or a thermalized Boltzmann distribution $P(J) \propto J^2 \exp(-BJ^2/k_B T)$. Work along these lines is presently in progress.

Acknowledgments

The authors wish to thank the GDR *Agrégats, Dynamique et Réactivité* for financial support.

¹ U. Ray, M. F. Jarrold, J. E. Bower, and J. S. Kraus, *J. Chem. Phys.* **91**, 2912 (1989).

² C. Bréchnignac, Ph. Cahuzac, J. Leygnier, and J. Weiner, *J. Chem. Phys.* **90**, 1492 (1989).

³ H. J. Hwang, D. K. Sensharma, and M. A. El Sayed, *Phys.*

Rev. Lett. **64**, 808 (1990).

⁴ S. Wei, B. Tzeng, and A. W. Castleman, Jr., *J. Chem. Phys.* **92**, 332 (1990).

⁵ J. A. Smith, N. G. Gotts, J. F. Winkel, R. Hallett, A. J. Stace, and B. J. Whittaker, *J. Chem. Phys.* **97**, 397 (1992).

- ⁶ C. X. Xu, D. A. Hales, and P. B. Armentrout, J. Chem. Phys. **99**, 6613 (1993).
- ⁷ U. Hild, G. Dietrich, S. Krückeberg, M. Lindinger, K. Lützenkirchen, L. Schweikhard, C. Walther, and J. Siegler, Phys. Rev. A **57**, 2786 (1998).
- ⁸ W. A. de Heer, K. Selby, V. Kresin, J. Masui, M. Vollmer, A. Châtelain, and W. D. Knight, Phys. Rev. Lett. **59**, 1805 (1987).
- ⁹ C. Bréchnignac, Ph. Cahuzac, N. Kébaili, J. Leygnier, and A. Sarfati, Phys. Rev. Lett. **68**, 26 (1992).
- ¹⁰ T. P. Martin, Phys. Reports **273**, 199 (1996).
- ¹¹ M. Schmidt, R. Kusche, W. Kronmüller, B. von Issendorff, and H. Haberland, Phys. Rev. Lett. **79**, 99 (1997).
- ¹² M. Schmidt, T. Hippler, J. Donger, W. Kronmüller, B. von Issendorff, H. Haberland, and P. Labastie, Phys. Rev. Lett. **87**, 203402 (2001).
- ¹³ F. Gobet, B. Farizon, M. Farizon, M. J. Gaillard, J. P. Buchet, M. Carré, P. Scheier, and T. D. Märk, Phys. Rev. Lett. **89**, 183403 (2002).
- ¹⁴ C. Bréchnignac, Ph. Cahuzac, B. Concina, and J. Leygnier, Phys. Rev. Lett. **89**, 203401 (2002).
- ¹⁵ S. Weerasinghe, F.G. Amar, Z. Phys. D **20**, 167 (1991); J. Chem. Phys. **98**, 4967 (1993).
- ¹⁶ P. Parneix, Ph. Bréchnignac and F.G. Amar, J. Chem. Phys. **104**, 983 (1996).
- ¹⁷ P. Parneix, F.G. Amar, and Ph. Bréchnignac, J. Phys. Chem. **239**, 121 (1998).
- ¹⁸ F. Calvo, J. Phys. Chem. B **105**, 2183 (2001).
- ¹⁹ D. H. E. Gross, Rep. Prog. Phys. **53**, 605 (1990).
- ²⁰ J. Pochodzalla *et al.*, Phys. Rev. Lett. **75**, 1040 (1995).
- ²¹ M. E. Fisher, Rep. Prog. Phys. **30**, 615 (1967).
- ²² W. J. Chesnavich and M. T. Bowers, J. Chem. Phys. **66**, 2306 (1977).
- ²³ O. K. Rice and H. C. Ramsperger, J. Am. Chem. Soc. **50**, 617 (1928); L. S. Kassel, J. Phys. Chem. **32**, 225 (1928).
- ²⁴ V. Weisskopf, Phys. Rev. **52**, 295 (1937).
- ²⁵ P. C. Engelking, J. Chem. Phys. **85**, 3103 (1986); **87**, 936 (1987).
- ²⁶ G. H. PESlherbe and W. L. Hase, J. Chem. Phys. **105**, 7432 (1996).
- ²⁷ C. Bréchnignac, Ph. Cahuzac, B. Concina, J. Leygnier, B. Villard, P. Parneix, and Ph. Bréchnignac, Chem. Phys. Lett. **335**, 34 (2001).
- ²⁸ J. Jellinek and D. H. Li, Phys. Rev. Lett. **62**, 241 (1989).
- ²⁹ D. H. Li and J. Jellinek, Z. Phys. D **12**, 177 (1989).
- ³⁰ J. Jellinek and D. H. Li, Chem. Phys. Lett. **169**, 380 (1990).
- ³¹ M.A. Miller and D.J. Wales, Mol. Phys. **89**, 533 (1996).
- ³² F. Calvo and P. Labastie, Euro. Phys. J. D **3**, 229 (1998).
- ³³ F. Calvo and E. Yurtsever, Phys. Lett. A **266**, 387 (2000).
- ³⁴ A. J. Stace, J. Chem. Phys. **93**, 6502 (1991).
- ³⁵ P. Pechukas and J. C. Light, J. Chem. Phys. **42**, 3281 (1965).
- ³⁶ C. E. Klotz, J. Phys. Chem. **75**, 1526 (1971).
- ³⁷ M. F. Jarrold, *Introduction to statistical reaction theories*, in Clusters of Atoms and Molecules I, edited by H. Haberland (Springer, Berlin), 1991.
- ³⁸ F. Calvo and P. Labastie, Chem. Phys. Lett. **247**, 395 (1995).
- ³⁹ R. S. Dumont, J. Chem. Phys. **95**, 9172 (1991); S. C. Smith, *ibid.* **97**, 2406 (1992).
- ⁴⁰ F. Calvo, J. Galindez, and F.-X. Gadéa, J. Phys. Chem. A **106**, 4145 (2002).
- ⁴¹ R. H. Swendsen and J.-S. Wang, Phys. Rev. Lett. **57**, 2607 (1986); G. J. Geyer, in *Computing Science and Statistics: Proceedings of the 23rd Symposium on the Interface* (American Statistical Association, New York, 1991).
- ⁴² A. M. Ferrenberg and R. H. Swendsen, Phys. Rev. Lett. **61**, 2635 (1988).
- ⁴³ J. Gspann and H. Vollmar, in *Rarefied Gas Dynamics*, 8th Symposium, edited by K. Karamcheti (Academic Press, New York, 1974), p. 261; in *Rarefied Gas Dynamics*, 11th Symposium, edited by R. Campargue (CEA, Paris, 1979), Vol. II, p. 1193.
- ⁴⁴ L. A. Girifalco, J. Phys. Chem. **96**, 858 (1992).
- ⁴⁵ F. Wang and D. P. Landau, Phys. Rev. Lett. **86**, 2050 (2001).
- ⁴⁶ F. Calvo, Mol. Phys. **100**, 3421 (2002).
- ⁴⁷ M. P. Allen and D. J. Tildesley, *Computer Simulations of Liquids* (Oxford, 1987).
- ⁴⁸ One angular momentum LJ unit equals $33.41\hbar$ for Argon.
- ⁴⁹ P. Parneix and Ph. Bréchnignac, Euro. Phys. J. D **13**, 43 (2001).